Update on single-screw expander geometry model integrated into an open-source simulation tool

2015 IOP Conf. Ser.: Mater. Sci. Eng. 90 012064

(http://iopscience.iop.org/1757-899X/90/1/012064)

Update on single-screw expander geometry model integrated into an open-source simulation tool

D. Ziviani[1], I. H. Bell[2], M. De Paepe[1], M. van den Broek[1]

[1]Department of Flow Heat and Combustion Mechanics - Ghent University - UGent, Sint-Pietersnieuwstraat 41, 9000 Gent, Belgium
[2]Aerospace and Mechanical Engineering Department, University of Liège, Campus du Sart Tilman B49, B-4000 Liège, Belgium

E-mail: davide.ziviani@ugent.be,ian.h.bell@gmail.com, martijn.vandenbroek@ugent.be, michel.depaepe@ugent.be

Abstract. In this paper, a mechanistic steady-state model of a single-screw expander is described with emphasis on the geometric description. Insights into the calculation of the main parameters and the definition of the groove profile are provided. Additionally, the adopted chamber model is discussed. The model has been implemented by means of the open-source software PDSim (Positive Displacement SIMulation), written in the Python language, and the solution algorithm is described. The single-screw expander model is validated with a set of steady-state measurement points collected from a 11 kWe organic Rankine cycle test-rig with SES36 and R245fa as working fluid. The overall performance and behavior of the expander are also further analyzed.

1. Introduction

In the optimization of organic Rankine cycle (ORC), there is an open question about the choice of the appropriate expansion device for different applications and working conditions. Because of their wide power range, overall efficiency and good part-load performance, screw expanders are considered one of the most promising technologies. However, challenges arise especially at the lower capacities where other positive displacement machines , e.g. scroll, rotary vane, spool, etc., are more cost-effective. Since the early developments in the 1930s, twin-screw compressors have been widely used in the refrigeration and process gas industries. The single-screw compressor (SSC) concept was developed in the 1960s by B. Zimmern [1]. Its configuration has a number of advantages over the twin-screw such as balanced loading of the main screw, higher volumetric efficiency, long working life, low vibrations and a simplified configuration. Single-screw machines also require less demanding lubricating conditions than twin-screw machines. Due to these characteristics, ORC systems based on single screw expander (SSE) have recently gained attention. In the literature, a number of studies are dedicated to model and characterize the performance of SSCs. However, many of the results are either incomplete with respect to the theory behind the machine design or reveal inconsistencies in the data provided (e.g.[2] and[3]). On the other hand, SSEs have only been investigated experimentally [4], but the experimental data published was limited to compressed air as working fluid, not realistic for ORC applications.

Nomenclature

C	Distance (m)
D	Diameter (m)
h	Specific Enthalpy (kJ/kg)
	Heat Transfer Coefficient (kW/m^2K)
i	Transmission Ratio (-)
L	Length (m)
m	Mass (kg)
$\dot{m}$	Mass Flow Rate (kg/s)
p	Pressure (kPa)
$\dot{Q}$	Heat Rate (kW)
T	Temperature (K)
u	Specific Internal Energy (kJ/kg)
v	Specific Volume (m^3/kg)
V	Volume (m^3)
$\dot{V}$	Volumetric Flow Rate (m^3/s)
$\mathbf{v}$	Velocity Vector (m/s)
w	Tooth width (m)
z	Number of Grooves or Teeth ()
α	Angle (rad)
β	Angle (rad)
	Expansion Ratio(-)
δ	Clearance (m)
ε	Effectiveness (-)
η	Efficiency (-)
θ	Rotation Angle (rad)
ω	Angular Speed (rad/s)
Ω	Angle (rad)

Subscript

CV	Control Volume
exp	expander
el	electric
d	discharge
eff	effective
f	fixed
g	groove
int	internal
is	isentropic
l	liquid
m	mechanical
meas	measured
nom	nominal
s	suction
sh	shaft
sr	screw rotor
sw	starwheel
th	theoretical
v	volume

The authors proposed a new mechanistic model of SSE with a preliminary validation [5] and additional experimental results were also discussed [6]. The main issues that have been pointed out were the profile generation method and the mathematical description of the SSE geometry. In this paper, the equations used for the profile generation are provided on the basis of the work published by Yang S-C [7]. Additional geometry aspects such as suction and discharge angles, sealing lines, swept volume calculation are further analyzed. The deterministic model is briefly described as well as the integration into the open-source software PDSim [8]. An 11 kWe SSE, shown in Fig. 1(a) with a 122 mm rotor is used as reference case. The expander has been tested with two working fluids, i.e. SES36 and R245fa, and the details of the experimental setup are presented in the companion paper [9].

2. Single-screw expander geometry description

The expansion process of the SSE occurs simultaneously on both sides of the rotor. The inlet flow is split in two parts to reach each of the inlet ports. During the suction process, Fig. 1(b), the groove is filled by working fluid until the left flank of the groove passes the right edge of the triangular -shaped port. At suction closure, the working fluid starts the expansion process, Fig. 1(c). When the right side of the engaged tooth begins to leave the groove, the discharge process occurs, Fig. 1(d). Reference studies about the geometry of SSE can be found in literature concerning SSC, for example [2, 10–12]. However, the formulation is not always comprehensive and many aspects are missing. In the following, a description of the principles behind the SSE design are highlighted and the symbols adopted are in accordance with the open literature in order to facilitate the reading. The geometric description of the SSE involves a large number of variables and parameters. In particular, it is possible to group the variables in three groups: independent, dependent and limit-set variables. Besides the variables, a number of empirical

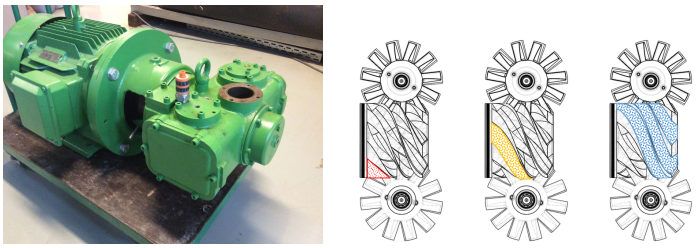

(a) (b) (c) (d)

Table 1. Geometric parameters of 11 kWe single-screw expander tested.

Engaging ratio	[-]	11/6
D_{sr}	[mm]	122
D_{sw}	[mm]	132
$V_{g,max}$	[cm^3]	57.39
$r_{v,built-in}$	[-]	4.7
L_{rotor}	[m]	121

Figure 1. (*a*) 11 kWe single-screw expander considered in the present study; Graphic representation of the single-screw expansion process: (*b*) suction; (*c*) closed expansion; (*d*) discharge. To be noted that the expansion process occurs simultaneously also on the opposite side of the rotor.

design parameters have to be selected. The independent variables include the number of grooves of main rotor, z_{sr}, the number of teeth of the starwheels, z_{sw}, the number of starwheels, N_{sw}, the main rotor diameter, D_{sr}, the starwheel outer and inner diameters, D_{sw}, $D_{sw,in}$ and the tooth width. The considered SSE has the standard configuration of 6 grooves in the main rotor and 11 teeth in the starwheels, which automatically defines the correlation between rotation angle and angular speed of the meshing pair:

$$i = \frac{z_{sw}}{z_{sr}} = \frac{\theta_{sr}}{\theta_{sw}} = \frac{\omega_{sr}}{\omega_{sw}} = \frac{11}{6}. \tag{1}$$

where ω_{sr} and ω_{sw} are the angular speed of main rotor and starwheel, respectively. The number of grooves typically is a multiple of the number of starwheels in order to balance the forces acting on the main rotor. In fact, the expansion or compression process will be symmetric in both sides of the rotor since the same number of grooves are engaged. It should be noted that the number of starwheels and their positions determine the type of configuration of the single screw machine, i.e. CC, CP, PC, PP [13]. The most common one is Cylinder-Plate (CP) and the reason behind it is explained in the following section dealing with the kinematics of meshing process. The number of teeth of the starwheel should not have a common factor with the number of grooves to guarantee the uniformity of the meshing and control the wear of the teeth. Increasing or decreasing the number of teeth has also the effect of modifying the swept volume [10]. The diameters of main rotor and starwheel are related by a design parameter, $D_{sw} = \lambda_d D_{sr}$. Normally, D_{sw} is either equal to or slightly larger (up to 10%) than D_{sr}. The diameter of the starwheel and the distance between the center axes of main rotor and starwheel, $d_{sr,sw}$ (in many cases $d_{sr,sw} = 0.8\, D_{sr}$) , influence the maximum groove volume and the degree of penetration of the tooth into the groove. The higher the degree of penetration and the higher the groove volume. However, there exists a maximum around 0.45$\sim$ 0.50 of penetration after which the width of the tooth has to be reduced in order to guarantee the structural integrity of the groove. For obvious reason there also is a structural limit related to the shaft diameter, $R_{sr} - (R_{sw} - R_{sw,in}) > R_{sr,sh}$. Dependent variables are related to the calculation of engaging angles and the length of the rotor sections. By referring to Fig. 2(a), it is possible to define:

$$\begin{aligned} \beta_s &= \cos^{-1}\left(\frac{d_{sr,sw} - R_{sr}}{R_{sw}}\right),\ \beta^* = \sin^{-1}\left(\frac{w}{2R_{sw}}\right) \\ \beta^*_{in} &= 2\sin^{-1}\left(\frac{w}{2R_{sw,in}}\right), \beta^*_{in} < \frac{2\pi}{z_{sw}} \end{aligned} \tag{2}$$

as well as:

$$L_{rot,eff} = L_s + L_d = R_{sw}\left(\sin\beta_s + \sin\beta_d\right)\ ,\ L^* = (0.1 \sim 0.15)D_{sr} \tag{3}$$

The selection of discharge angle β_d is related to the total engaging angle of the starwheel α_{sw} and typically $\beta_d = 0.7\,\beta_s$. The starwheel engaging angle and the corresponding groove wrap angle around the main rotor, α_{sr}, have an upper limit established by:

$$\alpha_{sr} = \alpha_{sw}\frac{z_{sw}}{z_{sr}} < \frac{2\pi}{N_{sw}} \tag{4}$$

Typically, $\alpha_{sw} \cong 90°$ and the explanation is given by the following relationship between the number of teeth engaged simultaneously, $n_{sw,eng}$, and the angular spacing of the teeth,γ:

$$\begin{aligned} &\alpha_{sw} = 2\beta^* n_{sw,eng} + 2.5\left(\gamma - 2\beta^*\right)\ ,\gamma = 2\pi/z_{sw} \\ &\alpha_{sw} = \beta_{open} + \beta_s + \beta^* \end{aligned} \tag{5}$$

where β_{open} represents the point of discharge opening. It is therefore a variable that defines a limit and determines how far the groove wraps around the rotor prior discharge. In other words, it influences the swept volume at the discharge angle and therefore the internal volume ratio. Finally, the tooth width is usually regarded as independent variable. The wider the tooth, the wider is the groove which results in an increased groove volume. However, there is a structural limit related to the minimum groove tip thickness, Δ. The analytic expression of the tooth width w, with the geometry and structural limits is given by:

$$\begin{aligned} &\Delta = \xi\, D_{sr},\ \xi = 0.017 \sim 0.025 \\ &w = 2\left(d_{sr,sw} - \frac{D_{sr}}{2}\right)\sin\frac{\gamma}{2} - \xi\, D_{sr}\,\cos\frac{\gamma}{2} \end{aligned} \tag{6}$$

A good approximation can also be obtained as $w \approx 0.3\,R_{sr}$. The geometric relationships can be developed on the basis of a reference system defined as in Fig. 2(a). In particular, a set of cylindrical coordinates (z, r, θ_{sr}) are positioned so that the z axis is coincident with the main rotor rotation axis and the r axis is perpendicular to the z axis and has its origin in correspondence of the perpendicular intersecting line from the starwheel rotation axis. A general point on the starwheel rotates in the z, r plane defined by the main rotor coordinates. On the starwheel an analogous reference system can be defined associated with the rotation angle θ_{sw} (see Fig. 2(a)).

3. Profile generation: direct problem of the main rotor

The geometry and kinematics of the SSE are directly linked and it is necessary to solve the groove profile generation in order to accurately describe the machine. From the fundamentals of gear kinematics, the single-screw type of meshing can be seen as a double meshing worm gear [14]. The conjugate worm gear surfaces rely on continuous contact lines that ensure the load-transmission. By transferring this concept to an expander (or compressor), the calculation of the contact lines and the precision during the manufacturing determine the sealing capabilities of the expansion (or compression) chamber. Generally, both the direct and indirect problems have to be solved [14]. In the following, only the direct problem, i.e. the cutting tool (tooth profile in this case) is given and the conjugated groove profile is calculated. The SSE considered in this study presents a single straight line meshing profile (SSLMP). From the gear kinematics theory [14], the meshing process of the screw rotor (sr) with two starwheels (sw) can be described as an envelope of two-parameter family of surfaces with a cylindrical-plate (CP) configuration. In particular, the generating surface is represented by the starwheel, i.e. plate, (direct problem). The profile

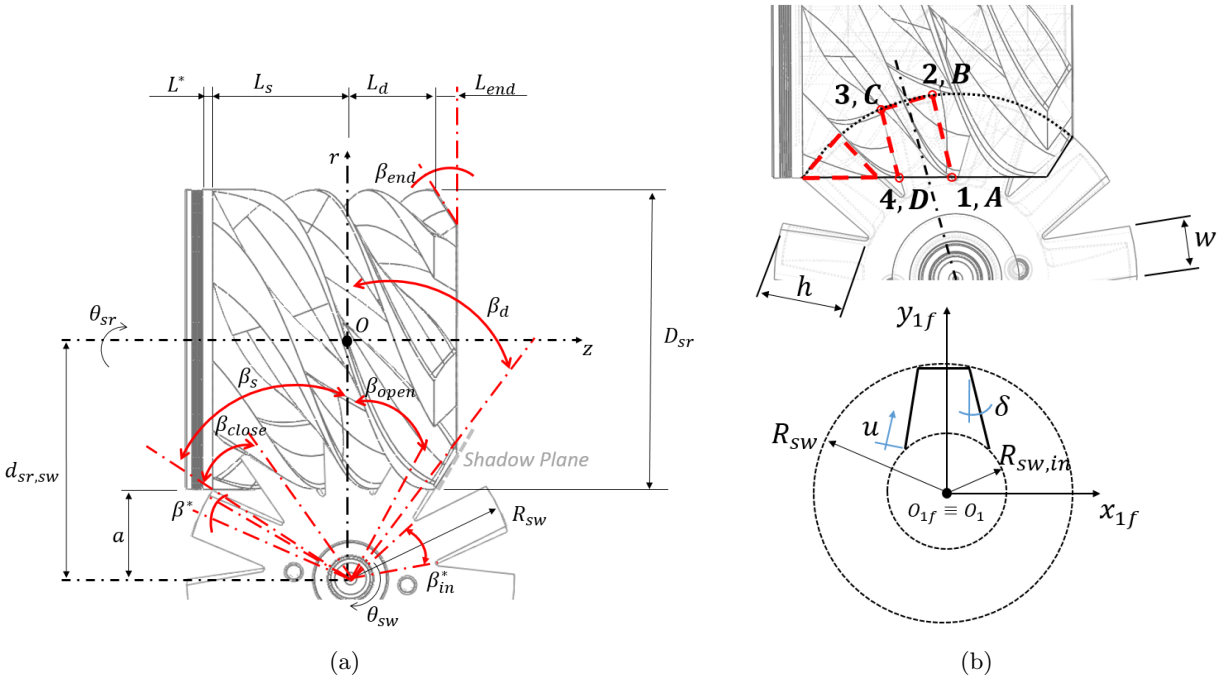

Figure 2. (a) Schematic of the main geometric parameters of the SSE; (b) description of a single engaging tooth into the mating groove.

of the starwheel is obtained by applying the inverse envelope concept. A right-handed fixed, $O_{i,f}(x_{if}, y_{if}, z_{if})$, and rotating, $O_i(x_i, y_i, z_i)$, coordinate systems have to be defined for both screw rotor ($i = 1$) and starwheel ($i = 2$). Each starwheel tooth engages the mating groove with three sides, identified by segments $\overline{AB}$, $\overline{BC}$ and $\overline{CD}$. The generic representation of a starwheel tooth is proposed in Fig. 2(b). A tooth with parallel flanks is obtained by fixing $\delta = 0$. Each segment of the tooth is described by a parameter u. The second parameter is the thickness of the tooth, t. By adapting the notation introduced in [14] and by applying the procedure described in [7], the system of coordinates in the screw rotor reference frame O_1 is given by:

$$\begin{cases} x_1 = -x_2 \sin\theta_{sw} \cos\theta_{sr} - y_2 \cos\theta_{sw} \sin\theta_{sr} + z_2 \cos\theta_{sr} + d_{sr,sw} \sin\theta_{sr} \\ y_1 = -x_2 \sin\theta_{sw} \cos\theta_{sr} - y_2 \cos\theta_{sw} \cos\theta_{sr} - z_2 \sin\theta_{sr} + d_{sr,sw} \cos\theta_{sr} \\ z_1 = x_2 \cos\theta_{sw} - y_2 \sin\theta_{sw} \end{cases} \tag{7}$$

where the relationship between θ_{sw} and θ_{sr} is given in (1). Eq. (7) can be further reworked to be used to generate the meshing curve. In particular:

$$\begin{cases} x_1 = -r \sin(\theta_{sr}) \cos(\theta_{sw} - \delta_u) + d_{sr,sw} \sin\theta_{sr} \\ y_1 = -r \cos(\theta_{sr}) \cos(\theta_{sw} - \delta_u) + d_{sr,sw} \cos\theta_{sr} \\ z_1 = -r \sin(\theta_{sr}) \cos(\delta_u - \theta_{sw}) \\ \delta_u = \pm \sin\left(\frac{w}{D_{sw}}\right) \\ r = \sqrt{\left(R_{sw} \cos\left(\sin^{-1}\left(\frac{w}{D_{sw}}\right) + h_{tooth}\right)\right)^2 + \frac{w^2}{4}} \end{cases} \tag{8}$$

The rotor is obtained through 3D cut-sweep by implementing Eq. 8 in a parametric form with the main rotor angular position as the running parameter. The meshing curve and the 3D model of the rotor are shown in Fig. 3(a).

4. Unwrapped groove curves and volume ratio calculation

At this point, having defined all the geometric parameters of the main rotor, it is possible to derive the helical equation of the groove in order to be able to represent it unwrapped on a plane [15]. A local reference system (Θ, z) is defined in order to obtain the 2D groove graphics where Θ is the unwrapped curvilinear coordinate of the rotor and z is the coordinate along the main rotor axis. In the (Θ, z), the extremities of each groove line have a distance equal to the wrap angle. Mathematically:

$$\begin{cases} \Theta = a\tan\theta_{sw} \pm \frac{w}{2\cos\theta_{sw}} & -\beta_{open} \leq \theta_{sw} \leq \alpha_r(\alpha_l) \\ z = R_{sw} i\left(\theta_{sw} + \beta_d\right), & \end{cases} \\ \alpha_r(\alpha_l) = \cos^{-1}\left(\frac{d_{sr,sw} - R_{sr}}{R_{sw}}\right) \pm sin^{-1}\left(\frac{w}{D_{sw}}\right) \tag{9}$$

where the $\pm$ sign is related to the subscripts r, $(+)$, and l, $(-)$, i.e. right and left sides of the groove, β_{open} is the opening angle which is influenced by the rotor end angle, β_{end}. The unwrapped groove is plotted in Fig. 3(c). The planar representation of the groove is necessary in order to calculate the sealing lines of the groove tips. The length of the groove tip leakage line at each main rotor angular position is given by,

$$L_{leak,tip} = \sum_{i\cdot\beta_s}^{\theta_{sr}} \sqrt{(\Delta\Theta)^2 + (\Delta z)^2} \tag{10}$$

Additionally, it can be used to estimate the internal built-in volume ratio. In fact, by introducing the real geometry of the suction port and its location, a crossing-algorithm can be implemented to recognize when the groove is crossing the suction port until suction closure, as shown in Fig. 3(d) and Fig. 3(e). Since the angle at which the discharge process begins can be calculated, β_{open}, the volume ratio can be determined. The correct estimation of the volume ratio allows to analyze the matching problem of the expander with the application. The evolution of the real suction port area, shown in Fig. 4(a),with respect the main rotor rotating angle is proposed in Fig. 4(b). A similar behavior can also be found in [10]. As a consequence, it is possible to optimize the suction process by investigating the shape and the area of the suction port. To be noted is that in Fig. 3(c), that at the current position of incipient discharge opening, the groove volume is not at its maximum. This is a characteristic of the single screw. By delaying the opening (β_{open}) it is possible to adjust the volume at discharge. In general, the swept volume can be defined as a function of D_{sr}^3, [2]. The swept volume is calculated by correlating the engaging tooth area into the corresponding groove and the tooth engaging angle. Generally, two approaches can be considered to obtain the engaging area, i.e. through a numerical integration of the tooth engaging area [16] or a polygonal approach which requires the definition of four corner points of a tooth at each rotation angle [12, 17]. A comparison between the different mathematical models of the groove volume is proposed in Fig. 4(b). To be noted that an analytic solution can be found by in integrating the function described in [16]. The numerical difference between the numerical integration and the analytic solution is negligible. However, the latter one reduces the overall computational time. A slight difference, around 3%, exists with respect to the polygonal approach. The polygonal description of the tooth is the adopted method to be included in the deterministic model because it allows the accurate calculation of the sealing lines on the tooth. The theoretical volume flow rate is given by:

$$\dot{V}_{th} = 2z_{sr}\frac{V_{g2}}{r_{v,builtin}}n. \tag{11}$$

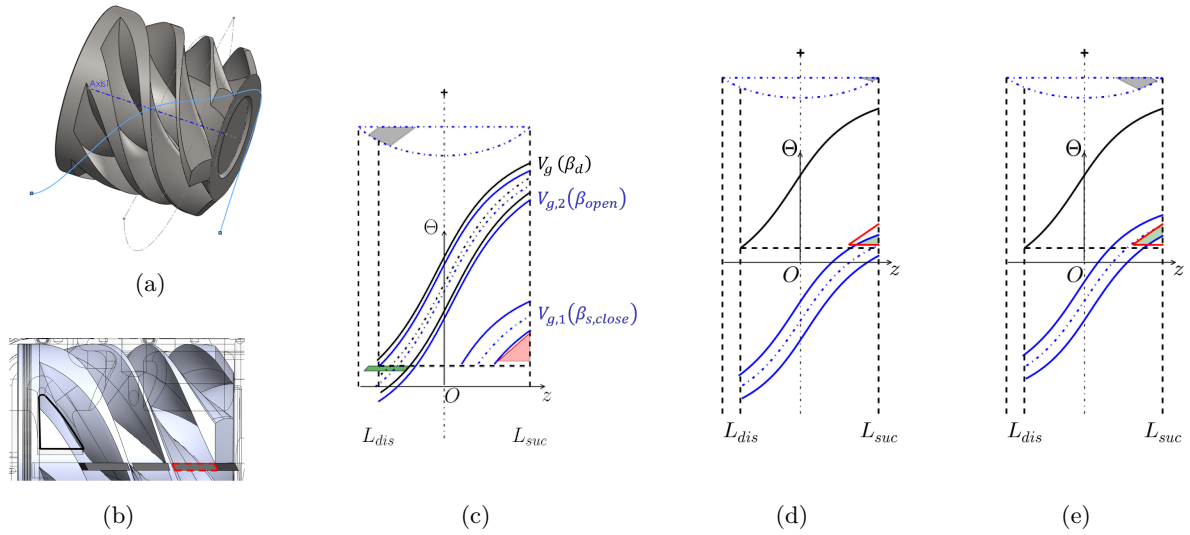

Figure 3. (a) Screw rotor profile generation in SolidWorks®; (b) 3D view of meshing condition at the beginning of the discharge, i.e. $\theta_{sw} = \beta_{open}$; (c) 2D representation of a groove where $V_{g,1} = V_g(\theta_{sw} = \beta_{s,closure})$,$V_{g,2} = V_g(\theta_{sw} = \beta_{open})$ and $r_{v,built-in} = V_{g,2}/V_{g,1}$; (d) Groove tip leading edge crossing the suction port; (e) groove tip trailing edge closing the suction port.

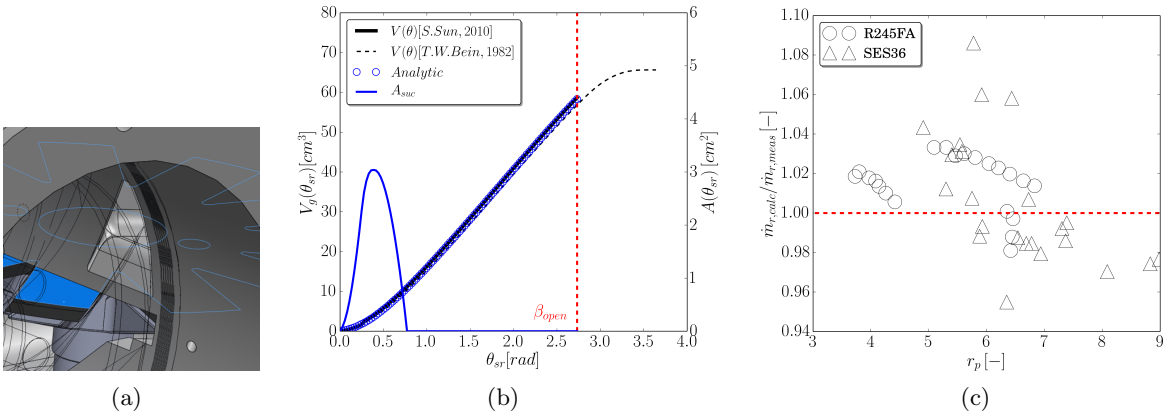

Figure 4. (a) 3D view of the suction port area; (b) Suction port area and comparison of different models for calculating the groove volume at each rotating angle of the main rotor; (c) Parity plot for calculated and measured values of mass flow rate for R245FA and SES36 .

5. Mechanistic model and Integration into PDSim

The mechanistic model is implemented by using a generalized framework for the simulation of positive displacement (PD) compressors and expanders, namely PDSim, developed by Bell [8]. The open-source software package[1] represents a useful tool that aims to overcome the non-availability of commercial software about mechanistic models of PD machines. PDSim has been developed in the Python programming language and its object-oriented structure allows to adapt the general core code to any PD compressor or expander. The basic idea is to integrate a geometry model specific for each machine into a general multi-chamber (or multi-control

[1] The PDSim website is at http://pdsim.sourceforge.net.

Table 2. Summary of the minimum and maximum measured values of the variables considered for both working fluids.

	Independent variables			Dependent variables			Performance indicators	
	$p_{su,exp}$ (kPa)	$p_{ex,exp}$ (kPa)	$T_{su,exp}$ (°C)	$\dot{m}$ (kg/s)	$\dot{W}_{el,exp}$ (W)	$T_{ex,exp}$ (°C)	$\eta_{is,sh,exp}$ (-)	ϕ_{FF} (-)
R245fa								
Min	566	120	106.7	0.12	1283	75.5	0.377	1.038
Max	1230	232	124.9	0.37	7364	104.6	0.624	1.331
SES36								
Min	450	90.7	91.65	0.150	903.8	73.99	0.542	0.897
Max	1028	177.9	125	0.406	7865	102.0	0.7232	1.117

volumes) approach based on a set of governing equations, standard flow models library, heat transfer and mechanical losses routines, as outlined in [5]. The analysis of a compressor or expander is based on a control volume approach which is representative of the internal working chamber. By assuming uniform temperature in the control volume, negligible kinetic energy and gravitational effects, thermal interaction through heat transfer, open control volume in terms of mass flow rate in and out, the conservation of mass and energy are imposed on the control volume. The thermo-physical properties of the working fluid are retrieved from the CoolProp library [18]. Due to the fact that the equations of state implemented are explicit in temperature and density, the governing equations have been expressed explicitly in terms of the derivative of temperature and density with respect the crack angle. For positive displacement machines, it is convenient to express the governing equations in terms of crank angle rotation rather than by time-dependent equations. The presence of lubricant oil (referred from now on as liquid) is accounted by assuming an homogeneous mixture. The additional state variable needed to fully describe a mixture of refrigerant and liquid has been chosen to be the liquid mass fraction, x_l. Therefore, the set of differential equations to be solved simultaneously for each control volume are the conservation of the total mass , the conservation of energy and the conservation of liquid mass. In particular, the conversation of energy is expressed in terms of $dT/d\theta$ and by recalling that $m_l = x_l \cdot m_{CV}$, it is possible to express the conservation of the liquid mass, m_l, in terms of the derivative of the liquid mass fraction with respect the crank angle, $dx_l/d\theta$. The complete mathematical derivation of the governing equations can be found in [19]. More details about the cycle solver algorithm can be found in [8].

6. Results and discussion

A total of 60 steady-state points have been determined from the experimental data for both R245fa and SES36. The description of the ORC test rig and the working fluid comparison have been presented in [6]. A specific analysis of the SSE with R245FA is proposed in a companion paper [9]. In Tab. 2, the minimum and maximum working conditions for both working fluids are listed. To be noted that only the electrical power output at the inverter was measured. However, by introducing the correlations for the inverter effectiveness and generator efficiency previously obtained [9], it has been possible to estimate the shaft power . Therefore,the expander isentropic efficiency at the shaft is defined as:

$$\eta_{is,sh,meas} = \frac{\dot{W}_{sh,calc}}{\dot{W}_{is,exp}} = \frac{\dot{W}_{el,meas}}{\eta_{mech,gen}\,\varepsilon_{el,inv}\,[\dot{m}_{meas}\,(h_{su,exp} - h_{ex,is,exp})]} \tag{12}$$

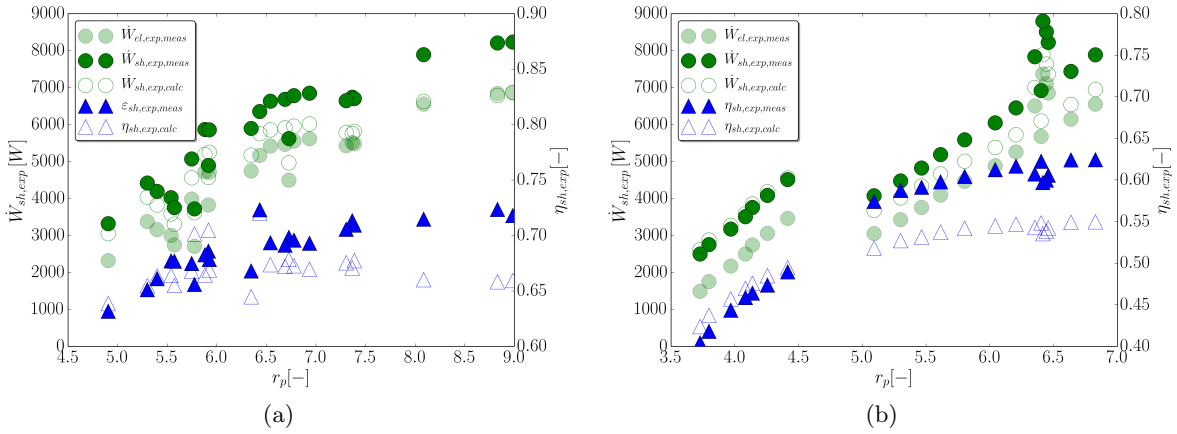

Figure 5. Comparison between predicted and measured shaft power and isentropic efficiency: (*a*) SES36; (*b*) R245FA.

In the following, the analysis of the experimental data is limited to the nominal rotational speed of 3000 rpm. The combination of the water-glycol air-cooled condenser and the thermophysical properties of the fluids have an impact on the overall performance. In particular, SES36 was tested during winter which allowed to have low condensing temperature and pressure with benefits on the power output and isentropic efficiency. R245fa presents a higher condensing pressure compared to SES36, and the spring conditions were not suitable to assess the maximum performance of the SSE. The tuning of the mass flow rate is mainly related to the leakage gap areas and the uncertainties associated to the non-perfect contact areas of the tooth flanks with the corresponding groove sides. Under the strong assumption that the leakage areas are constant, the mass flow rate is predicted within 3.5% for both fluids operating conditions, as shown in Fig. 4(c). By looking at the behavior of the mass flow rate relative errors at different pressure ratio, it is clear that the gaps vary with the operating conditions, typically due to rotor deformations, presence of oil and additional clearances during the meshing process. A correlation should be introduced to take into account rotational speed, pressure ratio. The predictions of the shaft power and the isentropic efficiency are more affected by inaccuracy, as shown in Fig. 5(a) and Fig. 5(b). Two source of errors can be identified: the measured shaft power is actually calculated by introducing generator and inverter performance maps since real measurements at the shaft were not available; the mechanical losses have been assumed to vary linearly with the rotational speed. The mechanical losses can be correctly estimated only if the flow irreversibilities and heat losses have been captured by the model. As a result, the shaft power has been predicted within 17% for both fluids. Slightly better convergence is obtained for R245FA with a mean relative error for the shaft power of 9.7%.

7. Conclusions

In this paper the geometry of a single-screw expander (SSE) has been analyzed in depth with emphasis on the profile generation and calculation of the main parameters. A 11 kWe SSE has been considered as test case and the geometry model has been validated with the real dimensions. The experimental performance has also been presented for two different fluids, i.e. SES36 and R245fa. Finaly, the geometry model has been integrated into a mechanistic model by using the open-source software PDSim.

Acknowledgment
The authors would like to thank Feilong Liu for his help in the understanding of the single-screw manufacturing process and profile generation design methods.

References

[1] Zimmern B and Patel G C 1972 Design and operating characteristics of the zimmern single screw compressor *International Compressor Engineering Conference* paper 16

[2] Sun G 1988 The investigation of some basic geometric problems of the single screw co *International Compressor Engineering Conference* paper 630

[3] Jin G, Zhang S and Yu X 2006 Theoretical analysis of diameter ratio of engagement pair for singe screw compressor *International Compressor Engineering Conference* paper 1831

[4] He W, Wu Y, Peng Y, Zhang Y, Ma C and Ma G 2013 *Applied Thermal Engineering* **51** 662 – 669

[5] Ziviani D, Bell I H, De Paepe M and van den Broek M 2014 Comprehensive model of a single screw expander for orc-systems applications *22th Int.Compressor Engineering Conf. at Purdue* 1506

[6] Gusev S, Ziviani D, Bell I H, De Paepe M and van den Broek M 2014 Experimental comparison of working fluids for organic rankine cycle with single-screw expander *Proceedings of 15th Int. Refrig. Air Cond. Conf. at Purdue* 2653

[7] Yang S C 2002 *Proceedings of IMechE, Part C: J. of Mechanical Engineering Science* **216** 343–351

[8] Bell I H, Lemort V, Groll E A, Braun J E and Horton W T 2013 Development of a generalized steady-state simulation famework for positive displacement ccompressor and expanders *Proceedings of 8th Int. Conf. on Compressors and their Systems, City University of London, London* pp 717–729

[9] Ziviani D, Desideri A, Lemort V, De Paepe M and van den Broek M 2015 Low-order models of a single-screw expander for organic rankine cyle applications *9th Int. Conf. on Compressors and their Systems, City University of London, London* 38

[10] Chan C Y, Haselden G G and Hundy G 1981 *Int. J. Refrigeration* **4** 275–280

[11] Bein T W and Hamilton J F 1982 Computer modeling of an oil flooded single screw air compressor *International Compressor Engineering Conference* paper 383

[12] Hirai T, Noda S, Sagara Y and Tsuzi K 1986 Performance analysis of oif single screw compressor *International Compressor Engineering Conference* paper 520

[13] Masuda M, Ueno H, Inoue T, Hori K and Hossain M 2013 Effact of variable volume index on performance of single screw compressor *Proceedings of 8th Int. Conf. on Compressors and their Systems, City University of London, London* pp 257–264

[14] Litvin F L 1994 *Gear Geometry and Applied Theory* (Prentice-Hall, New Jersey)

[15] Lundberg A and Gianvall R 1979 *Int. J. Refrigeration* **2** 221–232

[16] Sun S, Wu W, Yu X and Feng Q 2010 Analysis of oil film force in single screw compressor *International Compressor Engineering Conference at Purdue* 2024

[17] Ignatiev K M 2012 Approach to the numeric geometry analysis of positive displacement compressors, its application to a single screw compressor simulation and verification by experiment *International Compressor Engineering Conference* 2059

[18] Bell I H, Wronski J, Quoilin S and Lemort V 2014 *Ind. Eng. Chem. Res.* **53** 2498–2508

[19] Bell I H 2011 *Theoretical and Experimental Analysis of Liquid Flooded Compression in Scroll Compressors* Ph.D. thesis Purdue Univeristy